Isotopically nonstationary ^{13}C flux analysis of changes in *Arabidopsis thaliana* leaf metabolism due to high light acclimation

Fangfang Ma[a,1], Lara J. Jazmin[b,1], Jamey D. Young[b,c,2,3], and Doug K. Allen[a,d,2,3]

[a]Donald Danforth Plant Science Center and [d]Agricultural Research Service, US Department of Agriculture, St. Louis, MO 63132; and Departments of [b]Chemical & Biomolecular Engineering and [c]Molecular Physiology & Biophysics, Vanderbilt University, Nashville, TN 37235

Edited by Richard A. Dixon, University of North Texas, Denton, TX, and approved October 9, 2014 (received for review October 17, 2013)

Improving plant productivity is an important aim for metabolic engineering. There are few comprehensive methods that quantitatively describe leaf metabolism, although such information would be valuable for increasing photosynthetic capacity, enhancing biomass production, and rerouting carbon flux toward desirable end products. Isotopically nonstationary metabolic flux analysis (INST-MFA) has been previously applied to map carbon fluxes in photoautotrophic bacteria, which involves model-based regression of transient ^{13}C-labeling patterns of intracellular metabolites. However, experimental and computational difficulties have hindered its application to terrestrial plant systems. We performed in vivo isotopic labeling of *Arabidopsis thaliana* rosettes with $^{13}CO_2$ and estimated fluxes throughout leaf photosynthetic metabolism by INST-MFA. Plants grown at 200 μmol $m^{-2}s^{-1}$ light were compared with plants acclimated for 9 d at an irradiance of 500 μmol·m^{-2}·s^{-1}. Approximately 1,400 independent mass isotopomer measurements obtained from analysis of 37 metabolite fragment ions were regressed to estimate 136 total fluxes (54 free fluxes) under each condition. The results provide a comprehensive description of changes in carbon partitioning and overall photosynthetic flux after long-term developmental acclimation of leaves to high light. Despite a doubling in the carboxylation rate, the photorespiratory flux increased from 17 to 28% of net CO_2 assimilation with high-light acclimation (Vc/Vo: 3.5:1 vs. 2.3:1, respectively). This study highlights the potential of ^{13}C INST-MFA to describe emergent flux phenotypes that respond to environmental conditions or plant physiology and cannot be obtained by other complementary approaches.

isotopomer modeling | metabolic flux analysis | photosynthesis | ^{13}C-labeling | primary metabolism

Photosynthetic organisms assimilate more than 100 billion tons of carbon, ∼15% of the atmospheric total, each year and generate organic compounds for food and renewable chemicals (1). However, photosynthesis is a complex process that responds to heterotrophic tissue demands and environmental stimuli such as drought, temperature, and light intensity (2, 3). The light incident on the plant varies with intensities in the range of 0–2,000 μmol photons·m^{-2}·s^{-1} and can change dramatically because of passing clouds, shading, and the position of the sun. Thus, plants adjust light harvesting and carbon assimilation steps to accommodate many fluctuations, resulting in changes in plant morphology, physiology, and metabolism (4).

For 95% of all terrestrial plants (i.e., C3 plants), the reductive pentose phosphate (Calvin–Benson–Bassham, or CBB) cycle directly links light and dark reactions and sustains anabolic activities (5). RuBisCO (ribulose-1,5-bisphosphate carboxylase oxygenase) plays a central role in the cycle by carboxylating ribulose-1,5-bisphosphate (RUBP) with CO_2 to form two 3-phosphoglycerate (3PGA) molecules. The other 10 enzymes in the CBB cycle regenerate the RUBP substrate to repeat this process. RuBisCO has a low turnover rate (∼3/s; ref. 6) and also performs a competitive oxygenation side reaction that limits carboxylation activity. The binding of RuBisCO to oxygen produces 2-phosphoglycolate (2PG), and additional enzymatic steps, known collectively as photorespiration, are required to convert 2PG into 3PGA. Rectifying the oxygenase-based production of 2PG, which would otherwise be toxic, requires CO_2 release and consumes energy through photorespiration, thereby expending up to 50% of all fixed carbon (7) to maintain plant health (8). Researchers have attempted to augment RuBisCO's specificity and throughput (9), introduce nonnative forms of RuBisCO (6), increase the regenerative capacity of the CBB cycle (10, 11), and minimize metabolic costs associated with photorespiration (12). These studies produced mixed results, thus advocating for a more comprehensive, systems-level approach to enhance and/or redirect photosynthetic carbon flux.

In silico methods including kinetic (13) and stoichiometric (14–16) models can simulate metabolic network behavior and improve our mechanistic understanding of photosynthetic metabolism, but the predictions must be experimentally verified by other methods (17). We and others have used metabolic flux analysis (MFA) based on steady-state ^{13}C labeling studies to map the flow of carbon through the biochemical pathways of plant seeds (18–21) or cultured plant cells (22, 23), which exhibit extended periods of pseudosteady-state metabolism. However, leaves exhibit diurnal patterns of metabolism with limited metabolic steady states (24, 25). Furthermore, autotrophic tissues produce uniform steady-state ^{13}C-labeling patterns that are largely uninformative (26). Therefore, transient $^{13}CO_2$ labeling studies are necessary to quantify leaf metabolic fluxes.

Significance

To our knowledge, this is the first time that isotopically nonstationary ^{13}C flux analysis has been successfully applied to map photoautotrophic fluxes in a terrestrial plant system. Our analysis reveals alterations in photosynthetic carbon flux in response to high light acclimation. We provide a quantitative description of metabolism that accommodates acclimation and estimates changes in important fluxes that are difficult to measure. This study demonstrates a comprehensive approach to map the flow and fate of carbon within plant metabolic networks.

Author contributions: F.M., L.J.J., J.D.Y., and D.K.A. designed research; F.M., L.J.J., J.D.Y., and D.K.A. performed research; J.D.Y. and D.K.A. contributed new reagents/analytic tools; F.M., L.J.J., J.D.Y., and D.K.A. analyzed data; and F.M., L.J.J., J.D.Y., and D.K.A. wrote the paper.

The authors declare no conflict of interest.

This article is a PNAS Direct Submission.

Freely available online through the PNAS open access option.

[1]F.M. and L.J.J. contributed equally to this work.

[2]J.D.Y. and D.K.A. contributed equally to this work.

[3]To whom correspondence may be addressed. Email: doug.allen@ars.usda.gov or j.d.young@vanderbilt.edu.

This article contains supporting information online at www.pnas.org/lookup/suppl/doi:10.1073/pnas.1319485111/-/DCSupplemental.

A prior $^{13}CO_2$ labeling study by Szecowka et al. (27) applied kinetic flux profiling (KFP) to estimate net carbon fixation and photorespiration fluxes along with biosynthetic fluxes leading to sucrose, starch, trehalose, and myo-inositol in *Arabidopsis* rosettes under a single condition with illumination at 120 μmol·m^{-2}·s^{-1}. The KFP approach (28) uses a differential equation model to regress the trajectories of unlabeled mass isotopomer abundances (M0) and intracellular pool size measurements obtained for multiple ^{13}C-labeled metabolites, but without accounting for the distribution of higher mass isotopomers (M1, M2) observed. In contrast, isotopically nonstationary MFA (INST-MFA) is able to describe the full mass isotopomer distributions (MIDs) of measured metabolites, and is therefore capable of distinguishing flux contributions from different metabolic pathways based on the atomic rearrangements they produce. This approach provides enhanced flux resolution and does not require direct pool size measurements.

Previously, we applied ^{13}C INST-MFA to map 76 fluxes within the central carbon metabolism of the cyanobacterium *Synechocystis* sp. PCC 6803 (29). The flux analysis revealed unanticipated photosynthetic inefficiencies tied to oxidative metabolic pathways, despite minimal photorespiration. In this study, we applied a similar modeling approach to map autotrophic metabolism of *Arabidopsis* rosettes under varying light intensities by administering $^{13}CO_2$ to whole plants. ^{13}C INST-MFA was applied to determine (*i*) network-wide flux estimates from isotopomer labeling for both low light (LL) and high light acclimated (HL-ACC) *Arabidopsis* plants; (*ii*) a compartmentalized description of sucrose and starch biosynthesis; (*iii*) a description of leaf export of sucrose and amino acids consistent with measurements of vascular exudates; and (*iv*) model-based estimates of inactive pools consistent with cellular and subcellular leaf heterogeneity. The models were validated through benchmarking fluxes with the literature and by independent experiments not used for model identification. This study reveals the potential for ^{13}C INST-MFA to provide previously unidentified insights into photosynthetic metabolism that can guide plant metabolic engineering.

Results

Plant Development and Photosynthetic Rates. Developmental stages and photosynthetic metabolism are closely linked. Leaf morphology, pigmentation, photosynthetic rate, enzyme activities, and carbon partitioning impact plant development. In turn, the expansion of leaves, development of reproductive sink, and leaf senescence influence photosynthesis (30). Leaves of 3- to 5-wk-old *Arabidopsis* plants had comparable amounts of chlorophyll per unit of leaf fresh weight (FW) and net photosynthetic rates per unit of leaf area; however, RuBisCO content per unit FW decreased with age (Fig. 1, *Inset*), and 5-wk-old plants exhibited flower development. Fully expanded leaves of 4-wk-old plants were selected for all further experiments. Light–response curves (Fig. 1) indicated that plants acclimated to high light have ~38 ± 4% greater maximum photosynthetic rates than nonacclimated plants (measured at ~2,000 μmol·m^{-2}·s^{-1}) and an altered ratio of chlorophyll a/b (Fig. S1).

Starch and Sucrose Measurements. Starch and sucrose, two significant products of leaf photosynthetic metabolism, were quantified to determine the times during the day that leaves exhibit pseudosteady-state metabolism. The amount of starch and sucrose per unit FW were measured hourly from morning to midday. The leaves produced starch at a rate of 6.3 ± 0.3 μmol glucose·gFW^{-1}·hr^{-1} throughout the experimental time course (Fig. S1). The sucrose pool size did not change significantly during the same period, indicating that the biosynthetic and export rates were balanced. Therefore, plant leaves were isotopically labeled in the late morning.

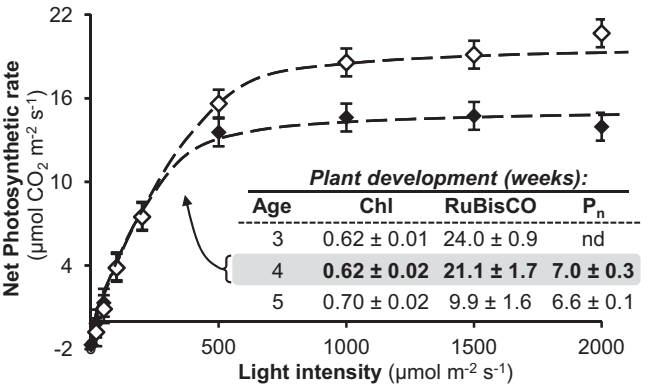

Fig. 1. Net photosynthetic rate as a function of light intensity in 4-wk-old plants. Plants were grown at light intensity of 200 μmol·m^{-2}·s^{-1} (black diamonds) or acclimated to 500 μmol·m^{-2}·s^{-1} for 9 d (white diamonds) before measurement (SEM; $n = 4$). (*Inset*) Photosynthetic measurements of leaves of 3- to 5-wk-old plants grown at 200 μmol·m^{-2}·s^{-1} including chlorophyll (Chl; mg·gFW^{-1}; SEM, $n = 4$), RuBisCO (mg·gFW^{-1}; SEM, $n = 3$), and net CO_2 assimilation rate (Pn; μmol CO_2·m^{-2}·s^{-1}; SEM, $n = 6$). Dotted lines are drawn to indicate trends.

^{13}C-Labeling of *Arabidopsis* Rosettes at Different Light Intensities. To map carbon fluxes after acclimation to varied light intensities, three to six replicate ^{13}C-labeling experiments were performed at low light (200 μmol·m^{-2}·s^{-1}; LL) or high light conditions after acclimation (500 μmol·m^{-2}·s^{-1}, 9-d acclimation; HL-ACC). Immediately after the introduction of ^{13}C-labeled CO_2, a time series of leaf samples were collected and the mass spectra of 37 fragment ions from each of 10 time points were analyzed by using LC-MS/MS and GC-MS (Dataset S1). The average ^{13}C enrichment of most metabolites increased hyperbolically over time, with the MID shifting gradually toward heavier mass isotopomers (Fig. 2 and Figs. S2 and S3). Intermediates involved in the CBB cycle, photorespiration, and sugar synthesis became enriched at a faster rate than organic and amino acids. Of the latter, only serine, glycine, alanine, and aspartate were significantly enriched during the initial 15-min labeling period.

ADP-Glucose and UDP-Glucose Reveal Metabolic Compartmentation. The MIDs of ADP-glucose (ADPG) and UDP-glucose (UDPG), which are the respective precursors for starch and sucrose biosynthesis, were examined to assess subcellular compartmentation in central metabolic pathways. Initial tests indicated labeling only within the glucosyl component of the nucleotide phosphates (Dataset S1); therefore, labeling was quantified only in this "metabolically active" component of ADPG and UDPG. Isotopic incorporation resulted in 81 ± 3% enrichment of ADPG and 49 ± 4% enrichment of UDPG at 15 min (Fig. 2*A*). The labeling differences confirm that starch and sucrose are generated from precursors that originate within distinct subcellular locations (i.e., plastid and cytosol, respectively, Fig. 2 *A* and *B*) and are consistent with current understanding of leaf carbon partitioning (31, 32).

Isotopically Nonstationary Metabolic Flux Analysis. A set of comprehensive isotopomer models were constructed to estimate metabolic fluxes based on the measured MIDs, the net CO_2 assimilation and starch production rates, and steady-state levels of sucrose and amino acids in vascular exudate (Fig. 3). The reaction network and fluxes (Fig. S4 and Dataset S1) included the CBB cycle, photorespiration, a bifurcated TCA pathway, and pathways for starch, sucrose, and amino acid biosynthesis (33). Inclusion of inactive pools and subcellular compartmentation was required to pass the χ^2 goodness-of-fit test and to describe

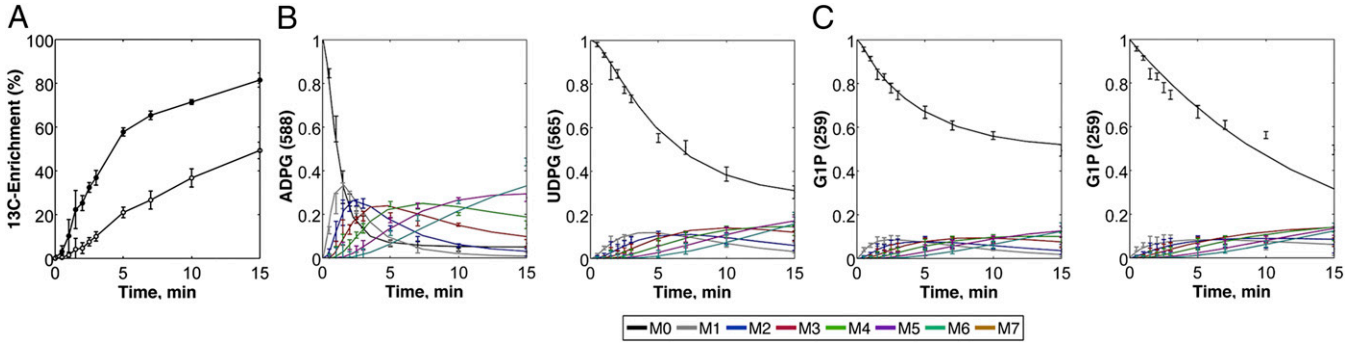

Fig. 2. Transient ^{13}C-labeling in intracellular metabolites. (*A*) Average ^{13}C-enrichments of ADP-glucose (ADPG; closed circles) and UDP-glucose (UDPG; open circles) under LL conditions calculated by using the formula $\left(\frac{1}{N}\right)\sum_{i=1}^{N} Mi \times i$, where *N* is the number of carbon atoms in the metabolite and *Mi* is the fractional abundance of the *i*th mass isotopomer. The solid lines connecting average ^{13}C enrichments were added to aid data visualization and do not represent model fits. (*B*) Experimentally measured mass isotopomer abundances (data points) and INST-MFA model fits (solid lines) of ADPG (*Left*) and UDPG (*Right*) under LL conditions. Error bars represent standard measurement errors (SEM, $n = 6$). Mass isotopomer data corrected for natural isotope abundance are shown. Nominal masses of M0 mass isotopomers are shown in parentheses for ADPG and UDPG. (*C*) Experimentally measured MIDs and INST-MFA model fits of glucose-1-phosphate (G1P) with (*Left*) and without (*Right*) inclusion of dilution parameters to account for inactive pools. Cellular heterogeneity can result in inactive pools that are not significantly enriched within the time course of the experiment. The contribution of these pools to the measured MID can be accommodated by incorporating dilution parameters into the model.

the multicellular, heterogeneous anatomy of a leaf (Fig. 2*C*). In general, the model-estimated sizes of inactive pools (expressed as a fraction of the total intracellular pool) were in qualitative agreement with M0 mass isotopomer abundances measured after a 60-min $^{13}CO_2$-labeling experiment (Fig. S5). Some quantitative disagreements were observed, most notably in the amino acid measurements collected under LL conditions, which were likely due to the existence of slowly labeled intracellular pools that were not explicitly included in the isotopomer model. These unmodeled pools appear inactive during the 15-min labeling experiment but become gradually enriched at longer times. Such discrepancies were less prevalent under HL-ACC conditions, likely because overall photosynthetic rates were enhanced and amino acid labeling equilibrated more rapidly.

TCA cycle metabolism is challenging to model in leaves because the combination of large organic acid pool sizes and low

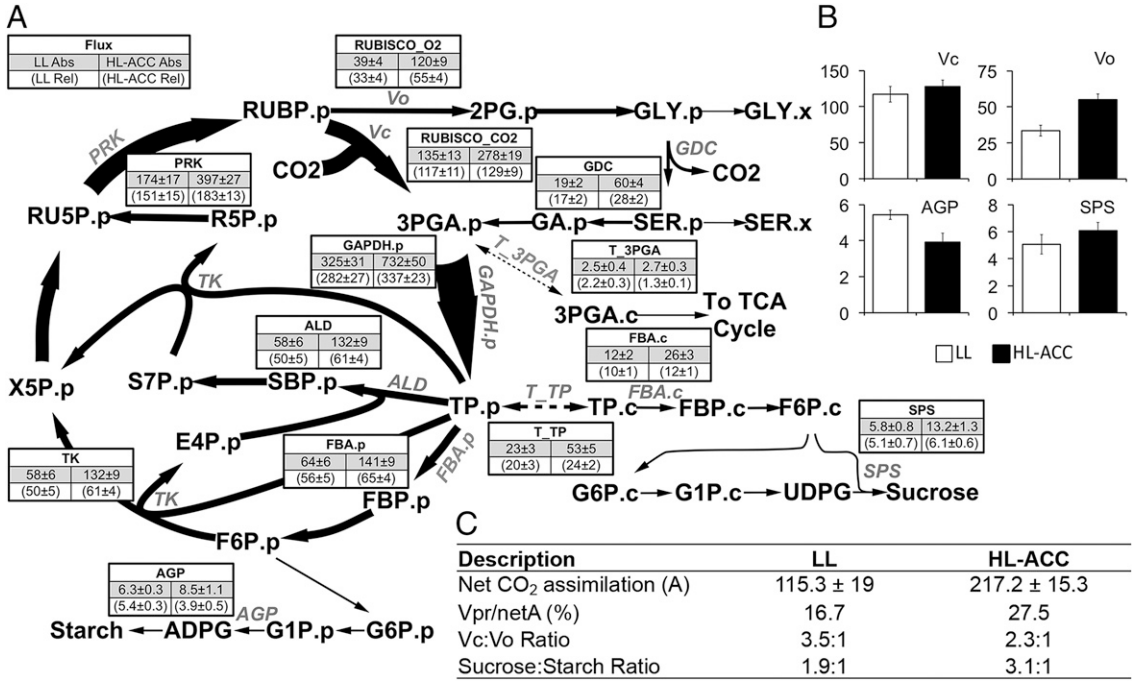

Fig. 3. Carbon assimilatory fluxes of a photosynthetic *Arabidopsis* leaf. (*A*) *Arabidopsis* net flux maps determined under varying light conditions for the LL and HL-ACC conditions. Relative fluxes are presented after normalization to a net CO_2 uptake rate of 100 (SEM, $n = 6$ LL; $n = 4$ HL-ACC). Values shown are the medians of the 95% flux confidence intervals. The estimated SEs are calculated as (UB95-LB95)/3.92, where UB95 and LB95 are the upper and lower bounds of each confidence interval, respectively, and 3.92 is the number of SEs that span the 95% confidence interval of a normally distributed random variable. Metabolites compartmentalized to the plastid are denoted by ".p," whereas metabolites compartmentalized to the cytosol are denoted by ".c." (*B*) Selected relative flux values (as a percentage of net CO_2 assimilation). (*C*) Comparison of photosynthetic parameters; net CO_2 assimilation is in terms of absolute fluxes (μmol metabolite·gFW^{-1}·hr^{-1}). AGP, starch synthesis flux; netA, net CO_2 assimilation; SPS, sucrose synthesis flux; Vc, carboxylation flux; Vo, oxygenation flux; Vpr, photorespiratory CO_2 release.

fluxes relative to CBB cycle (i.e., ~10% or less; ref. 33) result in poorly identifiable fluxes. To accurately depict the noncyclic TCA pathway activity, output fluxes to amino acids and sucrose were stoichiometrically constrained to each other on the basis of their measured steady-state concentrations in vascular exudate (Fig. S6). As an apoplastic loader, *Arabidopsis* can export more sucrose during high light acclimation because of H^+/sucrose symport (34, 35), which could result in an enhanced ratio of sucrose production relative to amino acids in HL-ACC plants.

Model-determined fluxes were not constrained to a particular measurement but rather were based on nonlinear regression of numerous MID measurements and experimentally derived starch and CO_2 net assimilation rates. Each model included 54 free flux parameters and required more than 1,000 ordinary differential equations (ODEs) to simulate the labeling time course of the measured MIDs (Fig. 3 and Figs. S2 and S3). Computing the sensitivities of all MIDs to the adjustable parameters required an additional ~94,000 ODEs. The LL and HL-ACC models had sum-of-squared residuals (SSR) of 1,003 and 808, which were both accepted based on χ^2 tests with degrees of freedom equal to 1,139 and 1,019, respectively (Fig. 3).

Metabolic Response to High Light Acclimation. Photosynthetic adjustments range from less than seconds to weeks or months dependent on the species and specific developmental process. This study focused on metabolic fluxes determined after 9 d of development with exposure to high light and was therefore aimed at examining the acclimated metabolic phenotype and not a short-term response to elevated irradiance. The 9-d time frame allowed plants to acclimate developmentally to a new metabolic pseudosteady state that was compared with LL leaves through the use of transient isotopic labeling experiments. The short time scale (~15 min) of the labeling experiments relative to time scale of acclimation enabled us to apply INST-MFA to obtain a snapshot of the flux values at the end of the acclimation period.

Absolute fluxes (μmol metabolite·gFW^{-1}·hr^{-1}) obtained from the best-fit models were subsequently normalized by the net assimilation rate to enable direct comparisons of carbon partitioning between LL and HL-ACC conditions (Fig. 3). Both the carboxylation and oxygenation activities of RuBisCO were established through the modeling process, resulting in a ratio of Vc/Vo that dropped from 3.5:1 in LL plants to 2.3:1 in HL-ACC plants. The change in this ratio reflected an absolute increase in photorespiratory flux from 19 to 60 μmol CO_2 released·gFW^{-1}·hr^{-1}, whereas carboxylation changed from 135 to 278 μmol CO_2 fixed·gFW^{-1}·hr^{-1}. As a result, photorespiratory fluxes were 17 and 28% of net assimilation, respectively. The additional carbon lost to photorespiration in the HL-ACC condition was offset primarily by decreases in the relative flux to starch accumulation (from 33 to 24% of net assimilation).

Despite the increase in photorespiration, the relative flux to sucrose export also increased to support more biomass production in HL-ACC plants. Sucrose export flux more than doubled from 11.7 to 26.4 μmol (hexose units)·gFW^{-1}·hr^{-1}, whereas starch production increased marginally from 6.3 to 8.5 μmol (hexose units)·gFW^{-1}·hr^{-1}. Higher carryover starch levels were observed in HL-ACC leaves throughout the diurnal cycle (Fig. S1). HL-ACC plants also had elevated levels of RuBisCO on the basis of leaf area, FW, or chlorophyll and produced thicker leaves with more biomass (Fig. S1). Furthermore, HL-ACC plants produced more seed biomass (i.e., 10 plants produced approximately twice the amount of seeds that resulted in 93% more biomass by weight) with a greater amount of oil, had altered leaf chlorophyll levels (Fig. S1), and had reduced measured concentrations of several of the Calvin cycle intermediates (Table S1).

Interestingly, measured changes in several CBB intracellular pool sizes were inversely correlated with the model-determined increase in CBB cycle fluxes for HL-ACC plants. We did not supply the pool size measurements to the model when performing data regressions because accurate measurement of absolute pool sizes can be challenging, and other methods aimed at indirectly assessing subcellular compartmentation (36, 37) were not applicable within the short time period of this study. As a result, most intracellular pool sizes were not identifiable by INST-MFA. Because pool size estimates were not strongly correlated to flux estimates (Figs. S7 and S8), precise determination of fluxes could still be achieved despite poor identifiability of pool sizes. This feature is a significant advantage of INST-MFA over other modeling approaches that do not use full MID measurements, require direct pool size measurements for data regression, or depend on kinetic parameter values that may not be reliably known *in planta*. We have observed a similar lack of coupling between flux and pool size estimates in previous studies (29), which appears to be a general characteristic of INST-MFA models.

Discussion

Leaf Metabolic Phenotyping by INST-MFA. INST-MFA provides a comprehensive approach to map the flow and fate of carbon throughout autotrophic metabolic networks (26). This method enables quantitative studies of integrated metabolic pathways, rather than individual reactions or nodes in isolation. Although INST-MFA has been previously applied to cultured cyanobacteria (29), this is the first time to our knowledge that it has been successfully performed in a terrestrial plant. Other recent studies have used $^{13}CO_2$ labeling to estimate fluxes (27) or metabolite turnover (38) from dynamic labeling data by modeling total ^{13}C enrichments, but without applying comprehensive isotopomer models. As presented here, isotopomer models that describe the full MIDs of the measured metabolites are capable of distinguishing flux contributions from different metabolic pathways based on the atomic rearrangements they confer. This approach allows increased pathway-specific information to be extracted from the MS measurements and, importantly, does not require direct pool size measurements to be supplied for model regression. The latter consideration is particularly germane to plant systems, because uncertainties introduced by metabolite compartmentation, rapid exchange with unmeasurable metabolites, heterogeneous cell populations, or losses during the extraction process may corrupt the absolute pool size measurements and lead to biased flux estimates when using previously established methods.

Although other models were considered based on biochemical descriptions in the literature, we found that dilution parameters to accommodate photosynthetically inactive metabolite pools were required to achieve statistically acceptable fits to the experimental data (Fig. S5), reflecting the cellular heterogeneity of leaves and also the mixing of compartmentalized pools that occurs during cell lysis. Incorporation of dilution parameters into the model enabled a parsimonious description of the labeling dynamics, which did not require detailed modeling of pools that cannot be independently measured and also did not depend on ad hoc assumptions found in the literature. The dilution parameters established by modeling were comparable to measurements obtained from a longer-term labeling experiment (t = 60 min), thus providing independent validation of this approach. Constraining the dilution parameters in the LL model to match the measured M0 isotopomer abundances at t = 60 min (with the exception of the amino acids alanine, serine, and glycine that label more gradually than the other metabolites included in the model), resulted in only a small increase in SSR from 1,003 to 1,087 and did not significantly alter the estimated flux values. Therefore, the change in SSR remained within statistically acceptable bounds and indicated that the estimated dilution parameters were in quantitative agreement with isotope labeling measurements at t = 60 min.

Photorespiration Changes with Acclimation to High Light. Methods to quantify photorespiration minimally include the following: postillumination CO_2 burst, inhibition of net CO_2 assimilation by O_2, CO_2 influx into CO_2-free air, NH_4 formation, and ratio of $^{14}CO_2$ to $^{12}CO_2$ uptake. The assumptions and limitations for each approach have been summarized (39, 40). We considered an alternative strategy using $^{13}CO_2$ labeling followed by computational flux estimation that does not require kinetic constants and, therefore, avoids some of the measurements and assumptions inherent to other methods. Furthermore, the approach (*i*) accounts for the exchange of intermediates across mitochondrial, peroxisomal, and cytosolic compartments (e.g., ref. 41) that interact with plastidic pools and (*ii*) couples photorespiration flux to biosynthetic demands for folate (42) and amino acid (43) metabolism. Thus, photorespiration is treated as a branched network with multiple input and output nodes, consistent with the known biochemistry.

Recent direct measurements of photorespiration indicate values of 14–17% of carboxylation (43, 44), consistent with the LL model; however, the range in the literature varies considerably (~6–70% photorespiratory CO_2 release relative to net assimilation). Our results indicate that the absolute rates of carboxylation and oxygenation increased with acclimation to high light intensity, but the rate of oxygenation increased more substantially (Fig. 3*B*). The HL-ACC case is not experimentally similar to a short-term exposure to high light because the additional acclimation time results in changes to leaf anatomy. In particular, HL-ACC plants have thicker leaves that maximize exposed chloroplast surface area to the intracellular space and swollen chloroplasts (Fig. S1) that contain heightened levels of RuBisCO per unit leaf area. Because the internal CO_2 conductance cannot increase in proportion to RuBisCO, leaves have greater internal diffusion resistances and lower CO_2 partial pressures at the site of carboxylation (45) that enhance photorespiration (46). Combining the ratio of model-derived Vo/Vc ratios for the LL and HL-ACC plants with gas exchange relationships that approximate photorespiration based on CO_2 concentration (39), the difference between LL and HL-ACC photorespiration would be explained by an additional 34% drawdown in the stromal CO_2 concentration at the carboxylation site C_c. This reduction is reasonable, because other studies on high light acclimation in leaves indicate up to 50% decrease in C_c (e.g., refs. 46 and 47).

Other parameters such as the enhanced levels of nucleotide cofactors that are cosubstrates in photorespiration may also further activate this pathway, rebalancing and consuming additional reducing equivalents across organelles and subverting photodamage (48). Photorespiration in HL-ACC plants led to consumption of an additional 72% ATP and 65% NADPH relative to the minimum required for CO_2 fixation, whereas in LL these percentages were lower (48% and 43%, respectively) but still significant.

Metabolism Adjusts in Light. The increase in photorespiratory carbon loss under the HL-ACC condition was associated with a repartitioning of flux among the major carbon sinks represented in the isotopomer model (Fig. 3). Relative flux to support sucrose export increased, whereas relative flux to starch decreased, indicating a higher carbon export capacity that corresponded to increased growth and photosynthetic flux in HL-ACC plants (35). The modeled sucrose to starch ratio (1.9:1) in LL plants was consistent with the literature and increased in HL-ACC plants to 3.1:1. Thus, the description of intermediary fluxes provided by INST-MFA enabled a global assessment of these flux alterations that would not be observable without a comprehensive, model-based analysis of isotope labeling dynamics.

This study also illustrates how combined analysis of flux and metabolite profiling data can provide complementary information about cellular reprogramming in response to light. For example, several measured metabolite intermediates appeared to adjust to the long-term high light acclimation through decreased pool sizes (on either a FW or chlorophyll basis) within the CBB cycle (Table S1), even as their interconnected pathway fluxes increased. Although this result was unanticipated, it was consistently obtained in multiple experiments by using sample collection strategies specifically designed to minimize shading or other potential artifacts.

The pool size measurements were not used in the INST-MFA model regressions, which provide an independent assessment of the metabolic adaptation to high light. Unfortunately, measured changes in metabolite levels could not be verified by INST-MFA, because the 95% confidence intervals for most model-estimated pool sizes exhibited overlap between the two conditions (Dataset S1). Furthermore, subcellular compartmentation and/or dilution by inactive pools will impact the model-estimated pool sizes but will not be reflected in the pool size measurements, thus complicating direct comparisons.

Although the inverse correlation between measured intermediate pool sizes and CBB cycle fluxes may seem counterintuitive from the standpoint of mass-action kinetics, it could be explained by increases in enzyme expression or other regulatory changes that occur during the acclimation process and is considered (49, 50). These longer-term physiological adaptations are not simply an extrapolation of the short-term response to high light. Further studies are needed to fully define the mechanism underlying this unexpected relationship between CBB cycle fluxes and intermediate pool sizes. However, this finding highlights the potential of ^{13}C INST-MFA to uncover systems-level properties of plant metabolic networks that are not directly observable by static metabolite profiling approaches.

Materials and Methods

Plant Growth Characteristics. Wild-type *Arabidopsis thaliana* ecotype Col-0 plants were grown in a Conviron growth chamber (model MTPS 120–2) under 16/8-h day/night cycles, temperature of 22/18 °C, light intensity of 200 $\mu mol \cdot m^{-2} \cdot s^{-1}$, and 50% relative humidity. At 24 d of age, plants were transferred to a Percival incubator (model E22L) that was set up with identical incubation conditions, where plants were maintained for 3 d before isotopic labeling (LL). For the high light acclimation process, plants initially grown to 17 d of age at 200 $\mu mol\ m^{-2} \cdot s^{-1}$ were exposed to 500 $\mu mol \cdot m^{-2} \cdot s^{-1}$ for 9 d before isotope labeling at 500 $\mu mol \cdot m^{-2} \cdot s^{-1}$ (HL-ACC). In both cases, plants were labeled 28 d after planting when leaves were fully expanded. Pigments including chlorophyll were quantified spectroscopically, RuBisCO was quantified by Western blot and gel image, sucrose was quantified by GC-MS, starch was quantified by using an enzymatic assay (Megazyme), leaf cross-sections and chloroplast ultrastructure were imaged in an energy filter transmission electron microscope (LEO 912 AB; LEO), and oil was quantified by gas chromatography flame ionization detection (GC-FID) (*SI Materials and Methods*).

Gas Exchange and $^{13}CO_2$ Labeling of *Arabidopsis* Rosettes. A LI-6400 XT portable photosynthesis system (Li-Cor) was used to monitor assimilation and light response of 4-wk-old plants. Isotopic labeling experiments ($n \geq 3$) were performed on plants acclimated to light intensities of 200 $\mu mol \cdot m^{-2} \cdot s^{-1}$ (LL) or 500 $\mu mol \cdot m^{-2} \cdot s^{-1}$ (HL-ACC). *Arabidopsis* rosettes were labeled in a Percival E22L incubator containing an inflated glove bag (Gas-Col) or custom-made individual gas-tight chambers, using premixed gas containing $^{13}CO_2$ (Sigma) at a $^{13}CO_2/N_2/O_2$ ratio of 0.033/78/21.967. Ten samples were collected over a 15-min interval at the following time points: 30, 60, 90, 120, 150, 180, 300, 420, 600, and 900 s followed by immediate quenching with liquid nitrogen. In each case, liquid nitrogen was dumped directly on plants that were still in the incubator with care to avoid any shading. The liquid nitrogen resulted in some leaves falling off of the rosettes almost instantly (i.e., less than 1 s after the nitrogen was applied). Therefore, we expect that the quenching process was adequate.

LC-MS/MS and GC-MS of Metabolite Labeling and Concentration. Methods to extract metabolites were modified from Arrivault et al. (24). Leaf tissue was extracted with methanol/chloroform/water (4 °C). Filtered samples were run on an AB Sciex QTRAP 4000 linked to a Shimadzu HPLC by using negative ionization. Ion-pair chromatography linked to tandem MS was performed as described in refs. 24 and 29 with slight modifications. GC-MS was used to inspect labeling in amino and organic acids (*SI Materials and Methods*).

Isotopomer Network and Flux Determination. An isotopomer model describing photosynthetic central carbon metabolism in *Arabidopsis* rosettes was constructed from reaction networks in biochemical literature. A list of the reactions, assumptions, and abbreviations is provided in *SI Materials and Methods*. INST-MFA was used to estimate intracellular metabolic fluxes. Least-squares parameter regression, and statistical and sensitivity analysis of the optimal solution, was performed by using the publically available software package Isotopomer Network Compartmental Analysis (INCA; ref. 51), which runs within MATLAB (19, 29). INCA relies on an elementary metabolite unit decomposition of the underlying isotopomer network to efficiently simulate the effects of varying fluxes on the labeling trajectories of measurable metabolites. Metabolic fluxes and pool sizes were estimated by minimizing the lack-of-fit between experimentally measured and computationally simulated MIDs by using a Levenberg-Marquardt optimization algorithm (52). Flux evaluation was repeated a minimum of 50 times from random initial values to obtain best-fit estimates. All results were subjected to a χ^2 statistical test to assess goodness of fit, and accurate 95% confidence intervals were computed for all estimated parameters by evaluating the sensitivity of the SSR to parameter variations (53).

ACKNOWLEDGMENTS. We thank Mr. James Gierse, and Drs. Howard Berg and Sarit Weissmann for technical help; the Proteomics and Mass Spectrometry and Integrated Microscopy Facilities at the Donald Danforth Plant Science Center where instrumentation was located; and helpful anonymous reviews and editorial comments. We acknowledge the following funding support: National Science Foundation Grant EF-1105249, Graduate Assistance in Areas of National Need Grant P200A090323, Department of Energy Grant DE-AC05-06OR23100, and the US Department of Agriculture, Agricultural Research Service.

1. Raines CA (2011) Increasing photosynthetic carbon assimilation in C3 plants to improve crop yield: Current and future strategies. *Plant Physiol* 155(1):36–42.
2. Eberhard S, Finazzi G, Wollman FA (2008) The dynamics of photosynthesis. *Annu Rev Genet* 42:463–515.
3. Paul MJ, Foyer CH (2001) Sink regulation of photosynthesis. *J Exp Bot* 52(360): 1383–1400.
4. Jänkänpää HJ, Mishra Y, Schröder WP, Jansson S (2012) Metabolic profiling reveals metabolic shifts in Arabidopsis plants grown under different light conditions. *Plant Cell Environ* 35(10):1824–1836.
5. Griffin KL, Seemann JR (1996) Plants, CO2 and photosynthesis in the 21st century. *Chem Biol* 3(4):245–254.
6. Sage RF (2002) Variation in the k(cat) of Rubisco in C(3) and C(4) plants and some implications for photosynthetic performance at high and low temperature. *J Exp Bot* 53(369):609–620.
7. Häusler RE, Hirsch HJ, Kreuzaler F, Peterhänsel C (2002) Overexpression of C(4)-cycle enzymes in transgenic C(3) plants: A biotechnological approach to improve C(3)-photosynthesis. *J Exp Bot* 53(369):591–607.
8. Maurino VG, Peterhansel C (2010) Photorespiration: Current status and approaches for metabolic engineering. *Curr Opin Plant Biol* 13(3):249–256.
9. Parry MA, et al. (2013) Rubisco activity and regulation as targets for crop improvement. *J Exp Bot* 64(3):717–730.
10. Miyagawa Y, Tamoi M, Shigeoka S (2001) Overexpression of a cyanobacterial fructose-1,6-/sedoheptulose-1,7-bisphosphatase in tobacco enhances photosynthesis and growth. *Nat Biotechnol* 19(10):965–969.
11. Henkes S, Sonnewald U, Badur R, Flachmann R, Stitt M (2001) A small decrease of plastid transketolase activity in antisense tobacco transformants has dramatic effects on photosynthesis and phenylpropanoid metabolism. *Plant Cell* 13(3):535–551.
12. Peterhansel C, Blume C, Offermann S (2013) Photorespiratory bypasses: How can they work? *J Exp Bot* 64(3):709–715.
13. Zhu XG, de Sturler E, Long SP (2007) Optimizing the distribution of resources between enzymes of carbon metabolism can dramatically increase photosynthetic rate: A numerical simulation using an evolutionary algorithm. *Plant Physiol* 145(2):513–526.
14. Boyle NR, Morgan JA (2009) Flux balance analysis of primary metabolism in Chlamydomonas reinhardtii. *BMC Syst Biol* 3:4.
15. Poolman MG, Kundu S, Shaw R, Fell DA (2013) Responses to light intensity in a genome-scale model of rice metabolism. *Plant Physiol* 162(2):1060–1072.
16. Grafahrend-Belau E, et al. (2013) Multiscale metabolic modeling: Dynamic flux balance analysis on a whole-plant scale. *Plant Physiol* 163(2):637–647.
17. Borisjuk L, et al. (2013) Seed architecture shapes embryo metabolism in oilseed rape. *Plant Cell* 25(5):1625–1640.
18. Lonien J, Schwender J (2009) Analysis of metabolic flux phenotypes for two Arabidopsis mutants with severe impairment in seed storage lipid synthesis. *Plant Physiol* 151(3):1617–1634.
19. Allen DK, Young JD (2013) Carbon and nitrogen provisions alter the metabolic flux in developing soybean embryos. *Plant Physiol* 161(3):1458–1475.
20. Alonso AP, Val DL, Shachar-Hill Y (2011) Central metabolic fluxes in the endosperm of developing maize seeds and their implications for metabolic engineering. *Metab Eng* 13(1):96–107.
21. Mandy DE, Goldford JE, Yang H, Allen DK, Libourel IGL (2014) Metabolic flux analysis using ^{13}C peptide label measurements. *Plant J* 77(3):476–486.
22. Masakapalli SK, Kruger NJ, Ratcliffe RG (2013) The metabolic flux phenotype of heterotrophic Arabidopsis cells reveals a complex response to changes in nitrogen supply. *Plant J* 74(4):569–582.
23. Sriram G, Fulton DB, Shanks JV (2007) Flux quantification in central carbon metabolism of Catharanthus roseus hairy roots by 13C labeling and comprehensive bondomer balancing. *Phytochemistry* 68(16-18):2243–2257.
24. Arrivault S, et al. (2009) Use of reverse-phase liquid chromatography, linked to tandem mass spectrometry, to profile the Calvin cycle and other metabolic intermediates in Arabidopsis rosettes at different carbon dioxide concentrations. *Plant J* 59(5): 826–839.
25. Hasunuma T, et al. (2010) Metabolic turnover analysis by a combination of in vivo 13C-labelling from 13CO2 and metabolic profiling with CE-MS/MS reveals rate-limiting steps of the C3 photosynthetic pathway in Nicotiana tabacum leaves. *J Exp Bot* 61(4):1041–1051.
26. Shastri AA, Morgan JA (2007) A transient isotopic labeling methodology for 13C metabolic flux analysis of photoautotrophic microorganisms. *Phytochemistry* 68(16-18):2302–2312.
27. Szecowka M, et al. (2013) Metabolic fluxes in an illuminated Arabidopsis rosette. *Plant Cell* 25(2):694–714.
28. Yuan J, Bennett BD, Rabinowitz JD (2008) Kinetic flux profiling for quantitation of cellular metabolic fluxes. *Nat Protoc* 3(8):1328–1340.
29. Young JD, Shastri AA, Stephanopoulos G, Morgan JA (2011) Mapping photoautotrophic metabolism with isotopically nonstationary (13)C flux analysis. *Metab Eng* 13(6):656–665.
30. Stessman D, Miller A, Spalding M, Rodermel S (2002) Regulation of photosynthesis during Arabidopsis leaf development in continuous light. *Photosynth Res* 72(1):27–37.
31. Zeeman SC, Smith SM, Smith AM (2007) The diurnal metabolism of leaf starch. *Biochem J* 401(1):13–28.
32. Stitt M, Lunn J, Usadel B (2010) Arabidopsis and primary photosynthetic metabolism - more than the icing on the cake. *Plant J* 61(6):1067–1091.
33. Tcherkez G, et al. (2009) In folio respiratory fluxomics revealed by 13C isotopic labeling and H/D isotope effects highlight the noncyclic nature of the tricarboxylic acid "cycle" in illuminated leaves. *Plant Physiol* 151(2):620–630.
34. Ainsworth EA, Bush DR (2011) Carbohydrate export from the leaf: A highly regulated process and target to enhance photosynthesis and productivity. *Plant Physiol* 155(1): 64–69.
35. Amiard V, et al. (2005) Anatomical and photosynthetic acclimation to the light environment in species with differing mechanisms of phloem loading. *Proc Natl Acad Sci USA* 102(36):12968–12973.
36. Allen DK, et al. (2014) Quantification of peptide m/z distributions from 13C-labeled cultures with high-resolution mass spectrometry. *Anal Chem* 86(3):1894–1901.
37. Allen DK, Laclair RW, Ohlrogge JB, Shachar-Hill Y (2012) Isotope labelling of Rubisco subunits provides in vivo information on subcellular biosynthesis and exchange of amino acids between compartments. *Plant Cell Environ* 35(7):1232–1244.
38. Huege J, et al. (2007) GC-EI-TOF-MS analysis of in vivo carbon-partitioning into soluble metabolite pools of higher plants by monitoring isotope dilution after 13CO2 labelling. *Phytochemistry* 68(16-18):2258–2272.
39. Sharkey TD (1988) Estimating the rate of photorespiration in leaves. *Physiol Plant* 73(1):147–152.
40. Busch FA (2013) Current methods for estimating the rate of photorespiration in leaves. *Plant Biol (Stuttg)* 15(4):648–655.
41. Timm S, et al. (2008) A cytosolic pathway for the conversion of hydroxypyruvate to glycerate during photorespiration in Arabidopsis. *Plant Cell* 20(10):2848–2859.
42. Collakova E, et al. (2008) Arabidopsis 10-formyl tetrahydrofolate deformylases are essential for photorespiration. *Plant Cell* 20(7):1818–1832.
43. Cegelski L, Schaefer J (2006) NMR determination of photorespiration in intact leaves using in vivo 13CO2 labeling. *J Magn Reson* 178(1):1–10.
44. Pärnik T, Ivanova H, Keerberg O (2007) Photorespiratory and respiratory decarboxylations in leaves of C3 plants under different CO2 concentrations and irradiances. *Plant Cell Environ* 30(12):1535–1544.
45. Evans JR (1999) Leaf anatomy enables more equal access to light and CO2 between chloroplasts. *New Phytol* 143(1):93–104.
46. Terashima I, Hanba YT, Tholen D, Niinemets Ü (2011) Leaf functional anatomy in relation to photosynthesis. *Plant Physiol* 155(1):108–116.
47. Hanba YT, Kogami H, Terashima I (2002) The effect of growth irradiance on leaf anatomy and photosynthesis in Acer species differing in light demand. *Plant Cell Environ* 25(8):1021–1030.
48. Foyer CH, Bloom AJ, Queval G, Noctor G (2009) Photorespiratory metabolism: Genes, mutants, energetics, and redox signaling. *Annu Rev Plant Biol* 60:455–484.
49. Kruger NJ, Ratcliffe RG (2009) Insights into plant metabolic networks from steady-state metabolic flux analysis. *Biochimie* 91(6):697–702.
50. Fell DA (2005) Enzymes, metabolites and fluxes. *J Exp Bot* 56(410):267–272.
51. Young JD (2014) INCA: A computational platform for isotopically non-stationary metabolic flux analysis. *Bioinformatics* 30(9):1333–1335.
52. Young JD, Walther JL, Antoniewicz MR, Yoo H, Stephanopoulos G (2008) An elementary metabolite unit (EMU) based method of isotopically nonstationary flux analysis. *Biotechnol Bioeng* 99(3):686–699.
53. Antoniewicz MR, Kelleher JK, Stephanopoulos G (2006) Determination of confidence intervals of metabolic fluxes estimated from stable isotope measurements. *Metab Eng* 8(4):324–337.